Earth and Planetary Science Letters ∎ (∎∎∎∎) ∎∎∎–∎∎∎

Contents lists available at SciVerse ScienceDirect

Earth and Planetary Science Letters

journal homepage: www.elsevier.com/locate/epsl

The influence of kinetics on the oxygen isotope composition of calcium carbonate

James M. Watkins [a,*], Laura C. Nielsen [b], Frederick J. Ryerson [c], Donald J. DePaolo [d,e]

[a] Department of Geological Sciences, University of Oregon, United States
[b] Department of Geological and Environmental Sciences, Stanford University, United States
[c] Lawrence Livermore National Laboratory, United States
[d] Earth Sciences Division, Lawrence Berkeley National Laboratory, United States
[e] Department of Earth and Planetary Science, University of California-Berkeley, United States

ARTICLE INFO

Article history:
Received 3 April 2013
Received in revised form
29 May 2013
Accepted 30 May 2013
Editor: T.M. Harrison

Keywords:
calcite
oxygen isotopes
equilibrium
kinetic
carbonic anhydrase
paleothermometry

ABSTRACT

Paleotemperature reconstructions rely on knowledge of the equilibrium separation of oxygen isotopes between aqueous solution and calcium carbonate. Although oxygen isotope separation is expected on theoretical grounds, the temperature-dependence remains uncertain because other factors, such as slow exchange of isotopes between dissolved CO_2-species and water, can obscure the temperature signal. This is problematic for crystal growth experiments on laboratory timescales and for interpreting the oxygen isotope composition of crystals formed in natural settings. We present results from experiments in which inorganic calcite is precipitated in the presence of 0.25 μM dissolved bovine carbonic anhydrase (CA). The presence of dissolved CA accelerates oxygen isotope equilibration between the dissolved carbon species CO_2, H_2CO_3, HCO_3^-, CO_3^{2-} and water, thereby eliminating this source of isotopic disequilibrium during calcite growth. The experimental results allow us to isolate, for the first time, kinetic oxygen isotope effects occurring at the calcite–water interface. We present a framework of ion-by-ion growth of calcite that reconciles our new measurements with measurements of natural cave calcites that are the best candidate for having precipitated under near-equilibrium conditions. Our findings suggest that isotopic equilibrium between calcite and water is unlikely to have been established in laboratory experiments or in many natural settings. The use of CA in carbonate precipitation experiments offers new opportunities to refine oxygen isotope-based geothermometers and to interrogate environmental variables other than temperature that influence calcite growth rates.

Published by Elsevier B.V.

1. Introduction

Paleotemperature reconstructions using biogenic and other natural carbonate minerals are based on equilibrium fractionation of oxygen isotopes between calcium carbonate and water. Equilibrium oxygen isotope fractionation is determined by the thermodynamic properties of the exchanging phases, but natural mineral growth typically occurs under non-equilibrium conditions, as does precipitation of calcite in laboratory experiments (Dietzel et al., 2009; Gabitov et al., 2012). Non-equilibrium oxygen isotope effects occur in the transfer of anions from solution to the growing crystal surface, and in the exchange of isotopes between dissolved CO_2 species and water. These non-equilibrium, or kinetic, effects are likely ubiquitous and therefore problematic for the interpretation of oxygen isotope ratios, as well as "clumped" isotope ratios, as paleotemperature indicators (Ghosh et al., 2006; Dietzel et al., 2009; Dennis and Schrag, 2010; Lachniet, 2009; Tripati et al., 2010).

Kinetic isotope effects are relatively well understood for Ca isotopes in calcite because the treatment of Ca isotopes is relatively simple; there is only one dissolved Ca^{2+} species in solution (DePaolo, 2011; Nielsen et al., 2012). Oxygen isotopes, on the other hand, have the complication that there are multiple dissolved oxygen-bearing carbonate species in solution, and if those species are not isotopically equilibrated, there is no way that the precipitated calcite can be in equilibrium. In this study, we use the enzyme, carbonic anhydrase, to achieve rapid oxygen isotopic equilibration among dissolved inorganic carbon species in the solution from which we precipitate calcite. This effectively eliminates the equilibration of the dissolved carbonate species as an uncertainty in measuring O isotope fractionation factors by experiment, allowing us to isolate non-equilibrium isotope fractionations arising at the mineral–solution interface.

We adapt a model that represents the effects of ion-by-ion growth of calcite to show how experimental measurements (almost certainly controlled by kinetics) can be reconciled with measurements of natural calcites formed under near-equilibrium conditions.

* Corresponding author. Tel.: +1 510 2255043.
E-mail address: watkins4@uoregon.edu (J.M. Watkins).

0012-821X/$ - see front matter Published by Elsevier B.V.
http://dx.doi.org/10.1016/j.epsl.2013.05.054

The model is based on the realistic assumption that ion attachment to, and detachment from, the calcite surface is mass dependent. The experimental results indicate that oxygen isotope-based paleothermometry works reasonably well because the kinetic fractionation factors, which describe oxygen isotope fractionation between calcite and dissolved carbon species, are relatively insensitive to temperature.

1.1. Background on oxygen isotopes and dissolved carbon species

The fractionation of oxygen isotopes between phases such as calcite and water is expressed in terms of a fractionation factor

$$\Delta^{18}O_{c-w} = 1000 \ln \alpha_{c-w}, \quad (1)$$

where

$$\alpha_{c-w} = \frac{[^{18}O/^{16}O]_{calcite}}{[^{18}O/^{16}O]_{water}}. \quad (2)$$

Values of $\Delta^{18}O_{c-w} > 0$ or $\alpha_{c-w} > 1$ indicate enrichment of the heavy isotope ^{18}O in calcite (c) relative to water (w). In carbonate crystal growth experiments, $\Delta^{18}O_{c-w}$ correlates with temperature, providing the basis for empirical calibrations of the oxygen isotope thermometer for inorganic and biogenic carbonates (Urey, 1947; McCrea, 1950; Epstein et al., 1953; O'Neil et al., 1969; Kim and O'Neil, 1997; Dietzel et al., 2009; Gabitov et al., 2012). Although carbonate isotope compositions are expressed relative to water, it has been suggested that the oxygen isotope fractionation between calcite and water is not controlled by calcite–water exchange, but by exchange between calcite and dissolved inorganic carbon ($DIC = [CO_2] + [H_2CO_3] + [HCO_3^-] + [CO_3^{2-}]$; brackets denote molar concentration) (Zeebe, 1999).

The relative abundance of DIC species depends primarily on *p*H, with a lesser dependence on temperature (Fig. 1a). At equilibrium, each DIC species exhibits its own temperature-dependent degree of ^{18}O enrichment relative to water (McCrea, 1950; Usdowski et al., 1991; Zeebe, 1999; Zeebe and Wolf-Gladrow, 2001; Beck et al., 2005). In fact, most of the temperature-dependence of ^{18}O in calcite, and its utility as a paleothermometer, can be attributed to the strong temperature-dependence of ^{18}O partitioning between DIC and water. An open question is whether the CO_3^{2-} groups incorporated into calcite are derived from the various dissolved species (Zeebe, 1999), whose proportions vary with temperature and *p*H, or strictly from the CO_3^{2-} ions, whose $^{18}O/^{16}O$ relative to H_2O is fixed for a given temperature regardless of *p*H (Watson, 2004; Dietzel et al., 2009). In either scenario, it is important to assess the kinetics of oxygen isotope exchange between DIC species and water during precipitation of calcite.

1.1.1. Uncatalyzed kinetics of ^{18}O exchange between CO_2(aq) and water

Direct exchange of oxygen isotopes between DIC and water occurs through CO_2 hydration and CO_2 hydroxylation reaction mechanisms (Zeebe and Wolf-Gladrow, 2001):

$$CO_2 + H_2O \underset{k_{-2}}{\overset{k_{+2}}{\rightleftharpoons}} H_2CO_3 \rightleftharpoons HCO_3^- + H^+ \quad (3a)$$

$$CO_2 + OH^- \underset{k_{-4}}{\overset{k_{+4}}{\rightleftharpoons}} HCO_3^- \quad (3b)$$

where the *k*'s are forward and backward reaction rate coefficients (Zeebe and Wolf-Gladrow, 2001). The hydration of CO_2 is the predominant reaction mechanism at low-*p*H, whereas at high *p*H the greater abundance of OH^- ions favors the hydroxylation reaction.

The time required for 99% ^{18}O equilibration between DIC and water is given by (Usdowski et al., 1991; Zeebe and Wolf-Gladrow, 2001; Uchikawa and Zeebe, 2012)

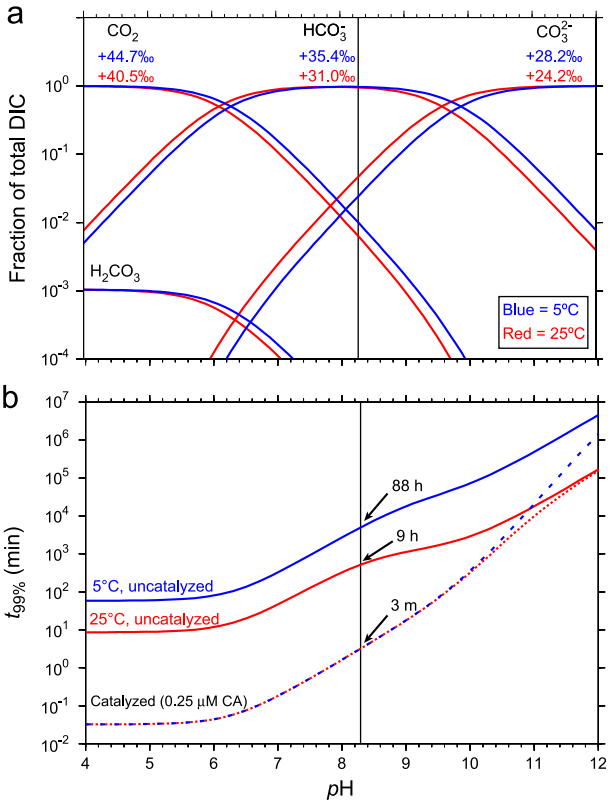

Fig. 1. (a) Speciation of dissolved inorganic carbon ($DIC = [CO_2] + [H_2CO_3] + [HCO_3^-] + [CO_3^{2-}]$) as a function of *p*H at 5 °C and 25 °C. Numbers under the species labels are permil enrichments in ^{18}O for each of the dissolved inorganic carbon species relative to water at 5 °C and 25 °C (Beck et al., 2005) and (b) solid lines show the time required to reach 99% equilibration ($\tau_{99\%}$) of oxygen isotopes among DIC species at 5 °C and 25 °C. Dashed lines show the calculated $t_{99\%}$ in the presence of 0.25 μM bovine carbonic anhydrase (CA), which is a catalyst for the hydration of dissolved CO_2.

$$t_{99\%} = -\ln(0.01)\tau, \quad (4)$$

where

$$\tau^{-1} = (0.5)\{k_{+2} + k_{+4}[OH^-]\} \times \left\{1 + \frac{[CO_2]}{S} - \left[1 + \frac{2}{3}\frac{[CO_2]}{S} + \left(\frac{[CO_2]}{S}\right)^2\right]^{0.5}\right\}. \quad (5)$$

Here, $S = [H_2CO_3] + [HCO_3^-] + [CO_3^{2-}]$. Eq. (5) states that the time required to achieve oxygen isotope equilibrium between DIC and water depends on the temperature-dependent forward reaction rate constants (k_{+2} and k_{+4}), and DIC speciation, which varies with temperature, salinity and *p*H. Fig. 1b shows $t_{99\%}$ versus *p*H using experimentally-determined k_{+2} and k_{+4} (Pinsent et al., 1956; Uchikawa and Zeebe, 2012). For HCO_3^- – dominated solutions, the timescales are hours to days, and for CO_3^{2-} – dominated solutions, the timescales are months to years. Although these timescales are short by geological standards, they are comparable to or greater than the duration of inorganic calcite growth experiments used to measure the equilibrium $\Delta^{18}O_{c-w}^{eq}$ (O'Neil et al., 1969; Kim and O'Neil, 1997; Dietzel et al., 2009; Gabitov et al., 2012). The kinetic parameters describing rates of ^{18}O exchange among dissolved species were not known until recently (Beck et al., 2005), but they suggest that previous calibrations of the ^{18}O calcite thermometer suffer from non-equilibrium effects due to incomplete exchange of ^{18}O between DIC and water, in addition to those due to crystal growth kinetics.

Please cite this article as: Watkins, J.M., et al., The influence of kinetics on the oxygen isotope composition of calcium carbonate. Earth and Planetary Science Letters (2013), http://dx.doi.org/10.1016/j.epsl.2013.05.054

1.1.2. Catalyzed kinetics of ^{18}O exchange between $CO_2(aq)$ and water

A way to reduce or eliminate kinetic oxygen isotope effects among DIC species is to introduce the enzyme carbonic anhydrase (CA), which catalyzes the inter-conversion of CO_2 and HCO_3^- via CO_2 hydration (Paneth and O'Leary, 1985; Uchikawa and Zeebe, 2012). The kinetic parameter that takes into account the catalyzed CO_2 hydration is (Uchikawa and Zeebe, 2012):

$$k^*_{+2} = k_{+2} + \frac{k_{Cat}}{k_M}[CA], \quad (6)$$

where k_{Cat} is catalytic rate constant and k_M is the Michaelis–Menten constant. The efficiency of bovine erythrocyte CA on the kinetics of ^{18}O equilibration among DIC was investigated by Uchikawa and Zeebe (2012) and the dashed curves in Fig. 1b show the expected, and quite dramatic, reduction in $t_{99\%}$ in the presence of just 0.25 μM dissolved CA. These curves were constructed assuming the catalyzed reaction rate constant k^*_{+2} is linearly dependent on the concentration of carbonic anhydrase (Uchikawa and Zeebe, 2012) and independent of temperature from 5 to 30 °C (Ghannam et al., 1986). If the DIC pool can reach ^{18}O equilibrium on a timescale much shorter than the timescale for crystal growth, any non-equilibrium ^{18}O uptake into calcite can reasonably be attributed to processes operating at or near the mineral–solution interface.

2. Calcite precipitation experiments

Inorganic calcite growth experiments were performed at pH = 8.3 with and without dissolved bovine erythrocyte CA to investigate (a) how and whether O isotopic disequilibrium between DIC and water influences the ^{18}O composition of inorganic calcite and (b) whether there are non-equilibrium isotope effects associated with the calcite precipitation reaction

$$Ca^{2+} + CO_3^{2-} \underset{k_-}{\overset{k_+}{\rightleftharpoons}} CaCO_3. \quad (7)$$

In our experiments, a beaker containing about 1300 mL of solution is placed inside a larger beaker that houses a temperature-controlled water bath. Fig. 2 shows a schematic of the experimental apparatus. The inner solution is prepared by dissolving salts of $CaCl_6 \cdot 2H_6O$ (30 mM), NH_4Cl (5 mM), and $SrCl_2 \cdot 6H_2O$ (0.1 mM) in deionized water. The NH_4Cl helps maintain fixed pH (cf. Tang et al., 2008a). The Sr is added to measure Sr partitioning into calcite, the results of which will be presented elsewhere along with calcium isotopes in calcite. Equations describing the chemical equilibria among dissolved species are provided in Appendix A.

The degree of supersaturation with respect to calcite ($\Omega = IAP/K_{sp}$, where IAP is the ion activity product and K_{sp} is the solubility product) is controlled by the composition and flow rate of a N_2+CO_2 gas mixture that is bubbled through the inner solution. In slow growth experiments Ω≈5, whereas in the fast growth experiments, Ω≈10. An important aspect of the experiment is that the ^{18}O composition of the gas differs significantly from that of the bulk solution. If CO_2–water isotopic exchange is incomplete, the precipitated calcite will inherit an isotopic composition that deviates significantly from the equilibrium value. By comparing results from experiments with and without the catalyst, the degree of DIC–water disequilibrium can be assessed.

2.1. Experimental run

Before an experiment begins, the gas mixture (pCO_2 = 200, 400, or 1000 ppmv) is bubbled into the solution through a diffusion stone (2 μm pores) at 0.500 standard cubic feet per hour (scfh) until the composition of the headspace matches the composition of the gas source. This usually takes about 30 min. To begin an experiment, the pH of the solution is brought up to the target value by NaOH addition. Throughout an experiment, the pH is monitored and controlled using a Multitasking titration system (Jensen Systems) interfaced with Titronic® universal burettes. We use an IoLine pH combination electrode (Schott® Instruments) calibrated with standard, NIST-traceable pH buffers.

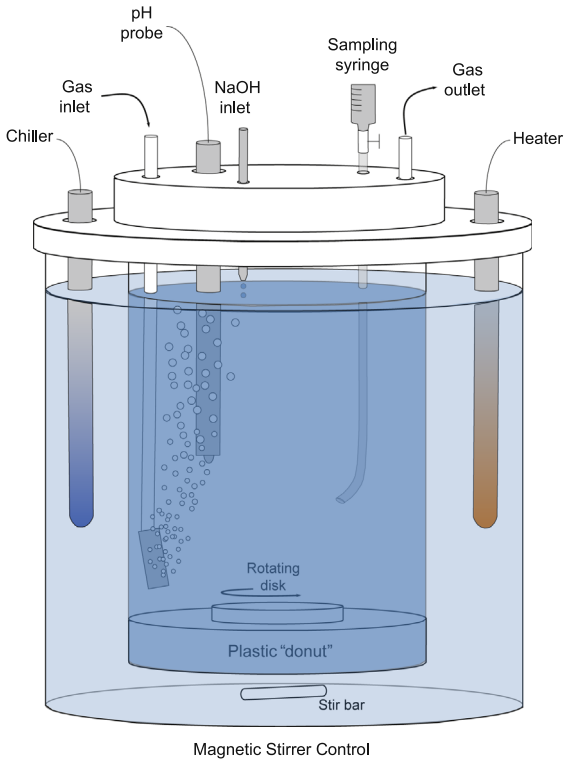

Fig. 2. Schematic of the experimental apparatus. The outer solution is a fixed temperature bath controlled by a chiller and heater. The inner solution (~1.3 L) contains dissolved salts of $CaCl_2$ (30 mM), $SrCl_2$ (0.1 mM), and NH_4Cl (5 mM). Dissolved inorganic carbon (DIC) is added to the inner solution by bubbling CO_2 at constant pH. The pH is maintained using an autotitration system with NaOH as the titrant. Once a critical supersaturation is reached, calcite crystals nucleate spontaneously and grow on the beaker walls and bottom. To maintain chemical homogeneity within the inner solution, a magnetic stir bar is implanted in a rotating disk held in place by a plastic "donut." The outer container rests on a magnetic stir plate. Several ports on the tops of the containers allow us to monitor and control chemistry throughout an experiment (see text).

The three panels of Fig. 3 show the output of a typical experimental run. Every experiment exhibits a similar behavior that can be divided into two stages. During Stage I, the rate of NaOH addition to solution reflects the rate of CO_2 addition in the absence of crystal growth. During Stage II, the rate of NaOH addition reflects the rate of CO_2 addition as well as the rate of calcite precipitation (Appendix B).

2.1.1. Stage I

Once the headspace composition matches that of the gas source, we send a command to the autotitrator to add NaOH until the pH hits a setpoint value of 8.3. This usually takes 2–5 min. The amount of NaOH needed to bring the pH up to 8.3 depends primarily on the amount of NH_4Cl dissolved in solution, but also on the initial $CO_2(aq)$ (note: this is why the Ω's are approximate). Upon increase of pH, additional CO_2 from the bubbles partitions into solution. The pCO_2 of the headspace is monitored throughout the experiment using a K-30 USB CO_2 Probe Data Logger (CM-0039 from CO2meter.com) with measurement range of 0–10,000 ppm and accuracy of ±5%. The typical behavior is shown in Fig. 3b. At the beginning of Stage I, the pCO_2 of the headspace decreases

Please cite this article as: Watkins, J.M., et al., The influence of kinetics on the oxygen isotope composition of calcium carbonate. Earth and Planetary Science Letters (2013), http://dx.doi.org/10.1016/j.epsl.2013.05.054

rapidly, indicating that roughly 1/2 to 3/4 of the gaseous CO_2 gets dissolved into solution. The pCO_2 of the headspace then gradually increases as the proportion of CO_2 added to solution decreases with time.

2.1.2. Stage II

The beginning of Stage II is characterized by an abrupt increase in the rate of NaOH addition due to the onset of calcite precipitation. This is very similar to the behavior described by Tang et al. (2008a) in their calcite precipitation experiments, but they did not report measurements of total alkalinity and did not have a headspace that could be used to make pCO_2 measurements. In our experiments, the increase in the rate of NaOH addition is accompanied by a decrease in the pCO_2 of the headspace, both of which are evidence for the onset of calcite precipitation. At the beginning of Stage II, the rate of NaOH addition increases, the pCO_2 of the headspace decreases, and the total alkalinity decreases. The decrease in pCO_2 implies that DIC is removed from solution faster than it can be supplied, indicating relatively rapid crystal nucleation and growth at high supersaturation. In a relatively short period of time, however, the system adjusts in such a way that the amount of CO_2 dissolving in solution is almost exactly balanced by the amount of CO_2 removed due to the precipitation of $CaCO_3$. In all of our experimental runs, and perhaps also the experimental runs of Tang et al. (2008a), the following quantities remain relatively constant during most of Stage II: (1) the rate of NaOH addition, (2) total alkalinity, (3) the rate of $[Ca^{2+}]$ removal (mmol/h), (4) the pCO_2 of the headspace, and (5) the degree of supersaturation. The ionic strength of the solution increases due to NaOH addition, but only by about 3%.

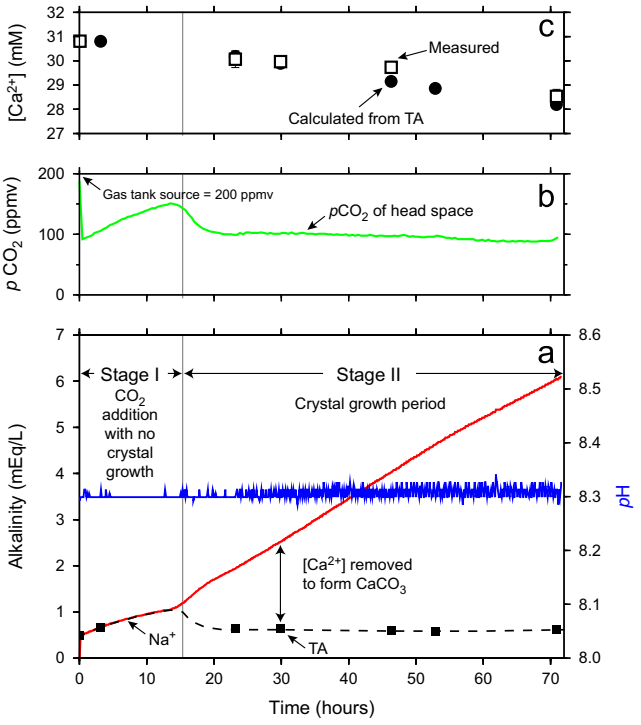

Fig. 3. Typical behavior during an experimental run. (a) Black squares = total alkalinity TA measured by titration of solution aliquots. Red = Alkalinity due to addition of NaOH. Blue = *p*H. During Stage I, the increase in TA matches the amount of NaOH needed to offset the addition of CO_2 to the solution. During Stage II, the change in TA is due to addition of NaOH as well as removal of Ca^{2+} to form $CaCO_3$, (b) evolution of the headspace pCO_2. An increase in the pCO_2 of the headspace indicates a decrease in the rate of CO_2 addition to the solution and (c) calculated $[Ca^{2+}]$ based on measurements of TA. During Stage II, $[Ca^{2+}]$ decreases while pCO_2 remains roughly constant.

2.2. Post-run analysis

After an experiment, the solution is vacuum filtered through Whatman 0.2 μm filter paper to collect any suspended crystals. The filtered solution is discarded. Most of the calcite crystals are adhered to the teflon cylinders and bottom of the beaker. Very few crystals are adhered to the sides of the beaker. Crystals are rinsed three times with 18.3 MΩ DDI H_2O and dried at room temperature under a fume hood. The crystals are gently scraped into three 7 mL savilex containers using a plastic wiper. About 3 mg are collected for $\delta^{(18/16)}O$ measurements and the rest (~50–100 mg) are saved for other measurements and future use. For experimental run products analyzed by XRD, calcite was confirmed as the sole phase. Fig. 4 shows characteristic scanning electron microscope (SEM) images of calcites grown. In most cases, crystals are rhombohedral but we did observe some scalenohedral crystals as well.

2.3. Growth rate

In many studies, crystal growth rates are cast in units of moles/m^2/s where m^2 refers to the reactive surface area. The reactive surface area is the most difficult parameter to quantify because it is scale-dependent and can increase (new crystals form) or decrease (existing crystals ripen) during an experiment. For direct comparison to previous results, we follow the approach of Tang et al. (2008a), and express the effective average surface area (SA) as the total reactive surface area at the time when half of the $CaCO_3$ has precipitated:

$$SA = \frac{Sp \cdot m}{2}, \tag{8}$$

where Sp is the specific surface area (m^2/g) and m is the total mass of calcite precipitated. In the experiments of Tang et al. (2008a), Sp was estimated using crystal size distributions (CSD) and a geometric model for rhombohedral calcite. The inferred Sp ranged from 0.2 to 0.5 m^2/g, with higher Sp for shorter experiments where the average crystal size was smaller. In most of their experiments, Sp was in the 0.27 ± 0.05 m^2/g range, so we use this value for comparison to their results and the results of Dietzel et al. (2009).

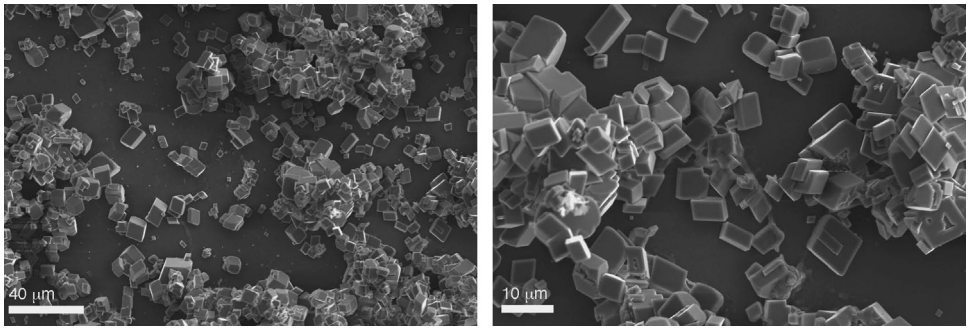

Fig. 4. SEM images of crystals.

Please cite this article as: Watkins, J.M., et al., The influence of kinetics on the oxygen isotope composition of calcium carbonate. Earth and Planetary Science Letters (2013), http://dx.doi.org/10.1016/j.epsl.2013.05.054

3. Measurements

3.1. Oxygen isotopes

Stable oxygen isotope compositions were measured at B.L. Ingram's Laboratory for Environmental and Sedimentary Isotope Geochemistry (LESIG) in the Department of Earth and Planetary Science, University of California-Berkeley. Aliquots containing about 10–100 μg of carbonate were used for oxygen isotope analyses. Measurements were collected on a GV IsoPrime mass spectrometer with Dual Inlet Multi-Carb system. The oxygen isotope compositions of solution aliquots were measuring using a Dual Inlet AquaPrep H_2O–CO_2 equilibrium method. Several replicates of three different standards were measured along with samples for each batch run. The oxygen isotope composition is expressed as

$$\delta^{(18/16)}O_{sample} = 1000\left[\frac{[^{18}O/^{16}O]_{sample}}{[^{18}O/^{16}O]_{standard}} - 1\right]. \quad (9)$$

The standard for carbonate samples is Pee Dee Belemnite (PDB) and the overall external analytical precision is better than ±0.07‰ for $\delta^{(18/16)}O_{calcite}$. The standard for water samples is Vienna Standard Mean Ocean Water (V-SMOW) and the overall external analytical precision is better than ±0.05‰ for $\delta^{(18/16)}O_{water}$. $\delta^{(18/16)}O_{calcite}$ values are recast relative to V-SMOW using the following conversion (Hoefs, 2009):

$$\delta^{(18/16)}O^{VSMOW}_{calcite} = 1.03086 \cdot \delta^{(18/16)}O^{PDB}_{calcite} + 30.86 \quad (10)$$

The relationship between δ values and the fractionation factor between calcite and water is given by

$$\alpha_{c-w} = \frac{\delta^{(18/16)}O^{VSMOW}_{calcite} + 1000}{\delta^{(18/16)}O^{VSMOW}_{water} + 1000} = \frac{(^{18}O/^{16}O)_{calcite}}{(^{18}O/^{16}O)_{water}} \quad (11)$$

Table 1 provides a summary of experimental conditions, inferred growth rates, and measured $\Delta^{18}O_{c-w}$ values.

4. Results and discussion

4.1. CA promotes homogeneous equilibrium in the bulk solution

The experiments without CA yield calcite crystals with variable oxygen isotope compositions at a given temperature and clearly far from oxygen isotopic equilibrium with the parent solution (Fig. 5). In stark contrast however, crystals grown in the presence of 0.25 μM CA exhibit ^{18}O compositions that are reproducible for a given temperature, and the temperature-dependence defines an approximately linear relationship that falls within the range of $\Delta^{18}O_{c-w}$ spanned by previous calibrations. The systematic relationship observed in the catalyzed experiments indicates that ^{18}O equilibrium between DIC and water has been achieved. In previous studies, it has been possible to show with quantitative precipitation experiments that barium carbonate has precipitated in the presence of an isotopically equilibrated DIC pool (Beck et al., 2005; Uchikawa and Zeebe, 2012), but this is the first direct evidence for DIC-water equilibrium during precipitation of calcium carbonate. Since the presence of CA does not appear to perturb the equilibrium ^{18}O partitioning among DIC species and water (Uchikawa and Zeebe, 2012), it is now possible to investigate ^{18}O uptake by calcite without experimental artifacts due to kinetic effects in the bulk solution. Our results also show that CA is an effective catalyst at low temperature (5 °C).

The relatively wide range in $\Delta^{18}O_{c-w}$ values from previous studies could have several origins. For example, there could be a solution composition-dependence to $\Delta^{18}O_{c-w}$; some studies are based on measurements of geological samples (Coplen, 2007; Chacko and Deines, 2008) or experiments at slow growth rates but in solutions of much higher ionic strength (Gabitov et al., 2012). Another issue is that in many experimental and natural settings, calcite crystals grow under conditions of variable *p*H (e.g., Kim and O'Neil, 1997), and it has been proposed that a *p*H-dependence on $\Delta^{18}O_{c-w}$ can explain why calcites precipitated at higher *p*H tend to have lower $\Delta^{18}O_{c-w}$ (Zeebe, 1999). Another important observation depicted in Fig. 5 is that cave calcites that precipitate over timescales of years to decades exhibit systematically higher $\Delta^{18}O_{c-w}$ values than experimentally precipitated calcites (Tremaine et al., 2011).

The study that is most directly comparable to the present is that of Dietzel et al. (2009), who grew calcites from a similar solution composition at fixed *T* and *p*H. Rather than supplying CO_2(g) from a gas source, CO_2(aq) was resupplied continuously by diffusion of CO_2(aq) from higher- and lower-*p*H sources through a plastic membrane to the experimental solution. Based on the timescales depicted in Fig. 1b, it is equivocal whether the data of Dietzel et al. (2009) represent ^{18}O disequilibrium among DIC

Table 1
Summary of experimental results.

Exp. number	CA[a] added?	pCO_2 (ppm)	Gas flow rate (scfh)	T[b] (°C)	t_1[c] (h)	t_2[d] (h)	M[e] (mmol)	log R[f] (mol/m²/s)	$\Delta^{18}O_{c-w}$[g] (‰)
2	No	200	~0.5	26.8	15	57	2.7	−6.44	22.71
3	No	400	~0.5	26.7	3	7	2.2	−5.53	17.74
4	No	1000	~0.5	26.7	3	5	2.3	−5.39	16.37
12	No	200	0.500	5	15	26	3.2	−6.10	17.27
13	Yes	400	0.500	5	12	11	2.4	−5.73	32.01
14	Yes	200	0.500	5	22	34	2.9	−6.22	32.40
15	Yes	200	0.500	15	16	38	2.5	−6.27	30.20
16	Yes	400	0.500	15	8	13	3.3	−5.80	30.15
17	Yes	200	0.500	25	5	38	3.3	−6.27	28.33
18	Yes	400	0.500	25	5	17	3.5	−5.92	28.10
P1	No	200	0.500	25	8	42	2.5	−6.31	–
P2	No	200	0.500	25	8	41	2.7	−6.30	–

[a] CA is from MP Biomedicals, lot nos. 8150K and M2724.
[b] Temperature is controlled to within ±0.3 °C.
[c] t_1 is the time elapsed prior to the onset of calcite nucleation.
[d] t_2 is the time elapsed during calcite precipitation.
[e] M is the amount of calcite precipitated.
[f] Reproducibility of R is within 0.05 log units based on two duplicated experiments P1 and P2. The uncertainty is somewhat larger, about 0.12 log units due to uncertainty in the specific surface area Sp (m^2/g) for calcite.
[g] Estimated uncertainty in $\Delta^{18}O_{c-w}$ is ±0.09‰.

Please cite this article as: Watkins, J.M., et al., The influence of kinetics on the oxygen isotope composition of calcium carbonate. Earth and Planetary Science Letters (2013), http://dx.doi.org/10.1016/j.epsl.2013.05.054

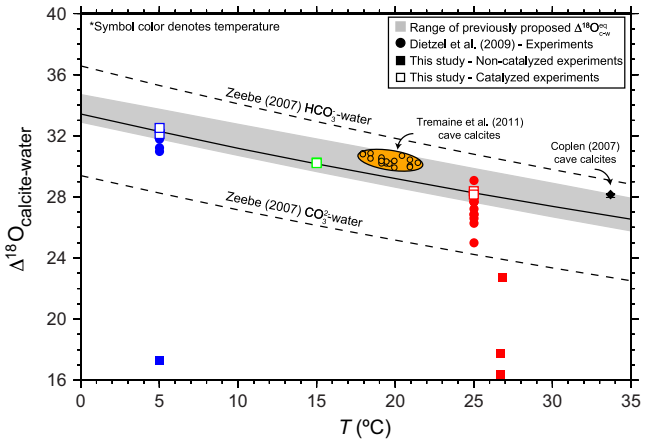

Fig. 5. Relationship between the observed oxygen isotope composition of calcite and temperature. The grey shaded area represents the range of proposed equilibrium values. The dashed lines show the equilibrium oxygen isotope composition of HCO_3^- and CO_3^{2-} relative to water. The solid line is parallel to the equilibrium CO_3^{2-}–water line to illustrate that nearly all of the temperature-dependence of oxygen isotope fractionation between calcite and water can be attributed to the temperature dependence of oxygen isotope fractionation between CO_3^{2-} (or HCO_3^-) and water. The temperature-dependence observed in the literature and in our catalyzed experiments does not necessarily imply oxygen isotope equilibrium between calcite and water. The data point from a natural cave calcite may represent thermodynamic equilibrium; it precipitated several orders of magnitude more slowly than experimental calcites (see Fig. 6).

species or disequilibrium between isotopically equilibrated DIC and calcite during precipitation, or a combination of these effects.

4.2. Kinetic effects due to precipitation

Even when the dissolved carbon species are in isotopic equilibrium, kinetic effects can also arise during precipitation and would be manifest in a dependence of the measured $\Delta^{18}O_{c-w}$ on precipitation rate (R). Our results show only a hint of a dependence on precipitation rate, but we did not sample a sufficiently large range in R to establish the functional form of this relationship. Fig. 6 shows $\Delta^{18}O_{c-w}$ versus R from uncatalyzed experiments of Dietzel et al. (2009) and our catalyzed experiments. The Dietzel et al. data, although somewhat scattered, imply a sign and magnitude of kinetic effects comparable to or slightly larger than what has been observed for Ca isotopes in calcite (Tang et al., 2008b). A somewhat smaller dependence of $\Delta^{18}O_{c-w}$ on R has been observed in a separate study using solutions of higher ionic strength (Gabitov et al., 2012).

The comparison to calcium is informative because the dependence of $\Delta^{(44/40)}Ca_{c-w}$ on R is better characterized (Tang et al., 2008b; DePaolo, 2011) and the equilibrium $\Delta^{(44/40)}Ca_{c-w}$ is constrained from calcites recrystallized in the presence of pore fluids over geologic timescales (Fantle and DePaolo, 2007). A key insight is that even at the slowest experimental growth rates, $\Delta^{(44/40)}Ca^{eq}_{c-w}$ inferred from nature has not been recovered (Tang et al., 2008b). For oxygen isotopes in calcite, the most convincing example of a crystal grown near thermodynamic equilibrium is a calcite vein that precipitated slowly in a natural cave setting at constant $T=33.7$ °C (Coplen, 2007). This crystal has higher $\Delta^{18}O_{c-w}$, by about 1.5‰, than would be inferred from the $\Delta^{18}O_{c-w}$–temperature relationship of our catalyzed experiments (Fig. 5). Based on this and the comparison to Ca isotopes, it is likely that neither ours nor any other experimental study has yielded the equilibrium value of $\Delta^{18}O_{c-w}$, which could be larger than the measured values by about 2‰.

4.3. Model for kinetic effects due to precipitation

To reconcile the observed kinetic effects with the equilibrium $\Delta^{18}O_{c-w}$ inferred from the slowly-precipitated natural cave calcite (Coplen, 2007), we have adapted an ion-by-ion attachment model previously developed to account for the pH dependence of precipitation rate (Wolthers et al., 2011), and the precipitation rate dependence of Ca isotopic fractionation between calcite and aqueous solution (Nielsen et al., 2012).

4.3.1. Calcite growth rate

Following Wolthers et al. (2011), we consider the growth of a calcite crystal via the incorporation of cations and anions to the kink sites and step edges of a cubic crystal (see Fig. 3 in Wolthers et al. (2011) for a schematic). The equation for calculating the rate of calcite growth is (Wolthers et al., 2011):

$$R_c = \frac{\rho_c u_c a^2 d}{y_0}, \tag{12}$$

where ρ_c is the steady state kink density (dimensionless), u_c is the kink propagation rate (s^{-1}), $a=3.199\times10^{-10}$ m is the closest spacing between adjacent Ca^{2+} and CO_3^{2-} sites on the calcite surface, $d=27{,}100$ moles/m^3 is the molar density of calcite, and y_0 (m) is the step spacing. The parameters ρ_c, u_c, and y_0 are functions of only a few input parameters given in Table 2. Table 3 lists all other depen dent parameters in an order that is convenient for calculating R_c. The shorthand notation is: $A_1=Ca^{2+}$ associated with CO_3^{2-}, $A_2=Ca^{2+}$ associated with HCO_3^-, $A=A_1+A_2$, $B_1=CO_3^{2-}$, $B_2=HCO_3^-$, and $B=B_1+B_2$.

4.3.2. Oxygen isotope discrimination

The isotopic composition of the solid is controlled by the net fluxes of heavy and light isotopes from the fluid to the solid phase (cf. DePaolo, 2011; Nielsen et al., 2012). Assuming a well-mixed fluid and neglecting diffusion (Zeebe, 2011), ion attachment to, and detachment from, kink sites controls the uptake of isotopes (Nielsen et al., 2012). The ratio r_c of $^{18}O/^{16}O$ in the calcite depends on the rates of $C^{16}O^{16}O^{18}O^{2-}$ and $HC^{16}O^{16}O^{18}O^-$ (B′) versus $C^{16}O_3^{2-}$ and $HC^{16}O_3^-$ (B) ion incorporation at kink sites (Nielsen et al., 2012):

$$r_c^* = \frac{u_{B'}}{u_B}, \tag{13}$$

where r_c^* represents the ratio of $C^{16}O^{16}O^{18}O^{2-}$ to $C^{16}O_3^{2-}$ in the crystal. We formulate the model using the singly-substituted species because it is the dominant ^{18}O-bearing species, but note that the model could be formulated in terms of $C^{18}O_3$. For the singly-substituted species, the fractionation factor will be

$$\alpha_{c-w} = \frac{\left(\frac{[^{18}O]}{[^{16}O]}\right)_c}{\left(\frac{[^{18}O]}{[^{16}O]}\right)_w} = \frac{r_c}{r_w} = \frac{1}{3}\frac{r_c^*}{r_w}. \tag{14}$$

The factor of 1/3 on the right-hand side is necessary for proper bookkeeping of oxygen isotope ratios cast in terms of oxygen atoms versus molecular CO_3 species (cf. Usdowski and Hoefs, 1993). Following Wolthers et al. (2011), the net rate of carbonate and bicarbonate ion uptake at kink sites on the calcite surface may be expressed as

$$u_B = u_{B_1} + u_{B_2} = k_{B_1}[B_1]P_A + k_{B_2}[B_2]P_A - \nu_{B_1}P_{B_1} - \nu_{B_2}P_{B_2}, \tag{15}$$

where the k's and ν's are rate coefficients for attachment and detachment, respectively, and P_A, P_{B_1}, and P_{B_2} are the probabilities of finding a calcium- or carbonate- or bicarbonate-terminated kink site. Equations used for the determination of kink site probabilities and rate coefficients are given in Table 3 and detailed in Wolthers et al. (2011). Eq. (15) can be rewritten in terms of effective

Please cite this article as: Watkins, J.M., et al., The influence of kinetics on the oxygen isotope composition of calcium carbonate. Earth and Planetary Science Letters (2013), http://dx.doi.org/10.1016/j.epsl.2013.05.054

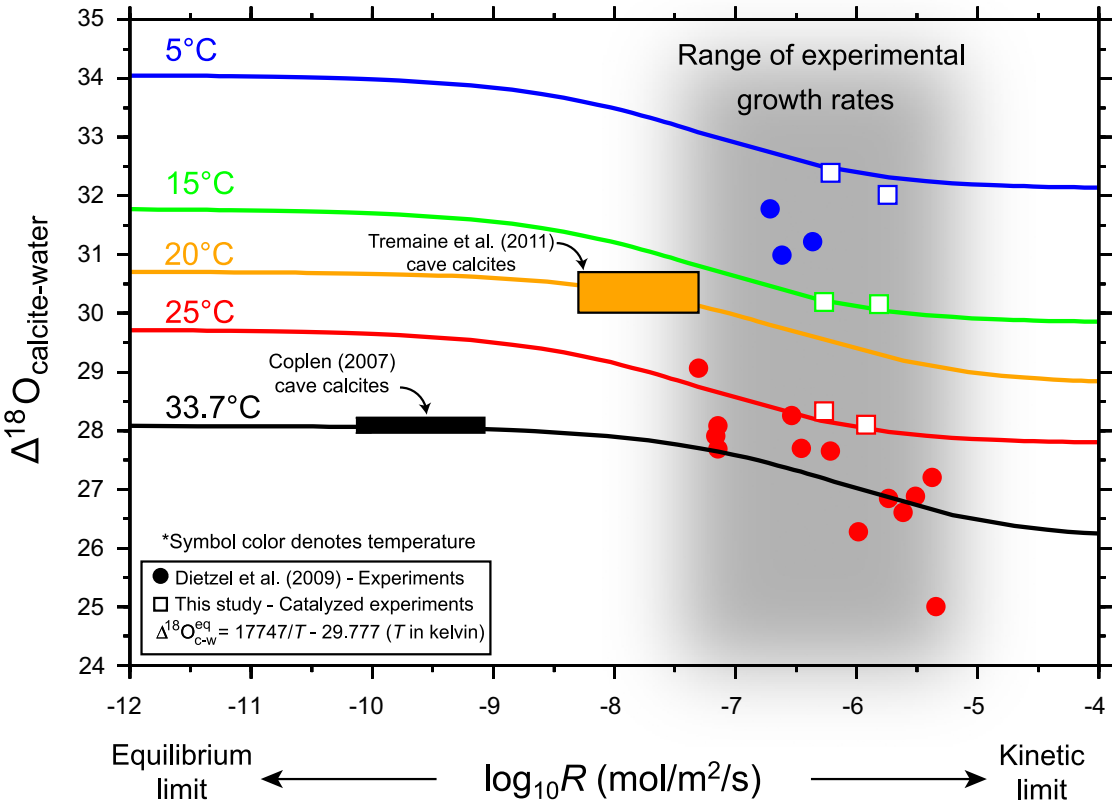

Fig. 6. $\Delta^{18}O_{c-w}$ versus precipitation rate R. The model curves describe the rate-dependence on $\Delta^{18}O_{c-w}$ while accommodating the equilibrium $\Delta^{18}O_{c-w}$ at 33.7 °C and pH=7.4 inferred from natural cave calcite (Coplen, 2007). The slowly grown cave calcites from Tremaine et al. (2011) formed at about 20 °C and pH≈7.8. In the model, the temperature dependence arises solely from temperature-dependent partitioning of oxygen isotopes between DIC species and water. The pH dependence arises from the difference in HCO_3^- versus CO_3^{2-} participating in calcite growth as a function of growth rate. The data of Dietzel et al. (2009) are isotopically light, which may be a consequence of isotopic disequilibrium among DIC species in the bulk solution from which calcite is precipitated. Such a disequilibrium effect is not incorporated into the model. An important insight from the agreement between model and data is that direct measurement of equilibrium $\Delta^{18}O_{c-w}$ by conventional methods may require experiments that last years to decades.

Table 2
Input parameters and values from Wolthers et al. (2011). Note that ν_{B_1} and ν_{B_2} need to be calculated after $\overline{\nu}_B$ in Table 3.

Parameter	Symbol	Value	Units
Kink formation energy	ϵ	6.7×10^{-21}	J
Edge work	γ	1.2×10^{-19}	J
Attachment frequencies	k_{A_1}	3.0×10^{6}	s^{-1}
	k_{A_2}	$\approx k_{A_1}$	s^{-1}
	k_{B_1}	$=2k_{A_1}\frac{1+10^{8.6}10^{-pH}}{1+10^{10.33}10^{-pH}}$	s^{-1}
	k_{B_2}	$\approx k_{B_1}$	s^{-1}
Detachment frequencies	ν_{A_1}	2×10^{3}	s^{-1}
	ν_{A_2}	$\approx\nu_{A_1}$	s^{-1}
	ν_{B_1}	$=\frac{K_S\overline{k}_A\overline{k}_B}{\overline{\nu}_A(1+10^{8.6}10^{-pH})}$	s^{-1}
	ν_{B_2}	$\approx\nu_{B_1}$	s^{-1}

attachment and detachment rate coefficients:

$$u_B=\overline{k}_B[B_1]P_A-\overline{\nu}_BP_{B_1}, \tag{16}$$

where

$$\overline{k}_B=k_{B_1}+\phi k_{B_2} \tag{17}$$

and

$$\overline{\nu}_B=\nu_{B_1}+\theta\nu_{B_2}. \tag{18}$$

In the above equations, θ is the ratio of HCO_3^-/CO_3^{2-} adsorbed on the calcite surface ($\approx10^{8.6}10^{-pH}$) and ϕ is the ratio of HCO_3^-/CO_3^{2-} in the bulk solution ($\approx10^{10.33}10^{-pH}$).

A similar expression to Eq. (15) can be written for the heavy isotopes of CO_3^{2-} (B'_1) and HCO_3^- (B'_2)

$$u_{B'}=u_{B'_1}+u_{B'_2}=k_{B'_1}[B'_1]P_A+k_{B'_2}[B'_2]P_A-\nu_{B'_1}P_{B'_1}-\nu_{B'_2}P_{B'_2}. \tag{19}$$

Expressions for $[B'_1]$ and $[B'_2]$ are taken from Beck et al. (2005), where

$$\alpha_{B_1-w}=\frac{\left(\frac{[^{18}O]}{[^{16}O]}\right)_{B_1}}{r_w}=\frac{1}{3}\frac{\left(\frac{[B'_1]}{[B_1]}\right)_w}{r_w}=\exp\left[\left(\frac{2,390,000}{T^2}-2.7\right)/1000\right], \tag{20}$$

and

$$\alpha_{B_2-w}=\frac{\left(\frac{[^{18}O]}{[^{16}O]}\right)_{B_2}}{r_w}=\frac{1}{3}\frac{\left(\frac{[B'_2]}{[B_2]}\right)_w}{r_w}=\exp\left[\left(\frac{2,590,000}{T^2}-1.89\right)/1000\right]. \tag{21}$$

In our model, all of the temperature dependence on $\Delta^{18}O_{c-w}$ arises from changes in the oxygen isotope distribution between aqueous CO_3^{2-} and HCO_3^-. The dependence of $\Delta^{18}O_{c-w}$ on precipitation rate arises from the statement that rate coefficients for B′ ion attachment and detachment do not equal those of B (DePaolo, 2011; Nielsen et al., 2012). To quantify this effect, it is convenient to define a forward (f) and backward (b) kinetic fractionation factor

Table 3
Parameters calculated from input parameters.

Parameter	Symbol	Value	Units
Fraction of kink sites suitable for growth	χ	1	No units
Closest spacing between A and B sites	a	3.199×10^{-10}	m
Molar density of calcite	d	27,100	moles/m^3
Solubility product for calcite	K_s	$\approx10^{-8.48}$	No units
Saturation ratio for calcite	S	$\left(\frac{[A][B_1]}{K_s}\right)^{1/2}$	No units
Rate coefficient for A attachment	$\overline{k}_A$	$k_{A_1}+10^{8.6}10^{-pH}k_{A_2}$	s^{-1}
Rate coefficient for B_1 and B_2 attachment	$\overline{k}_B$	$k_{B_1}+10^{10.33}10^{-pH}k_{B_2}$	s^{-1}
Rate coefficient for A detachment	$\overline{\nu}_A$	$\nu_{A_1}+\nu_{A_2}$	s^{-1}
Rate coefficient for B_1 and B_2 detachment	$\overline{\nu}_B$	$\nu_{B_1}+10^{8.6}10^{-pH}\nu_{B_2}$	s^{-1}
Probability that a given site is a B_1 site	P_{B_1}	$\frac{\overline{k}_B[B_1]+\overline{\nu}_A}{\overline{k}_A[A]+\overline{\nu}_B+(1+10^{8.6}10^{-pH})(\overline{k}_B[B_1]+\overline{\nu}_A)}$	No units
Probability that a given site is an A site	P_A	$1-(1+10^{8.6}10^{-pH})P_{B_1}$	No units
Probability that a given site is a B_2 site	P_{B_2}	$1-P_A-P_{B_1}$	No units
Net incorporation rate of A ions	u_A	$\overline{k}_A[A]P_{B_1}-\overline{\nu}_AP_A$	s^{-1}
Net incorporation rate of B ions	u_B	$\overline{k}_B[B_1]P_A-\overline{\nu}_BP_{B_1}$	s^{-1}
Net kink propagation rate	u_c	u_A+u_B	s^{-1}
Rate of kink formation on B sites	i_A	$2\exp\left(\frac{-2\varepsilon}{kT}\right)(S^2-1)\left(\frac{\overline{\nu}_B\overline{k}_A[A]}{\overline{k}_A[A]+\overline{\nu}_B}\right)$	s^{-1}
Rate of kink formation on A sites	i_B	$2\exp\left(\frac{-2\varepsilon}{kT}\right)(S^2-1)\left(\frac{\overline{\nu}_A\overline{k}_B[B]}{\overline{k}_B[B]+\overline{\nu}_A}\right)$	s^{-1}
Net rate of kink formation	i_c	$\frac{i_A+i_B}{2}$	s^{-1}
Steady state kink density	ρ_c	$\left(\frac{2i_c}{u_A+u_B}\right)^{1/2}$	No units
Step spacing	y_0	$\frac{19a\gamma}{kT\ln S}$	m
Calcite growth rate	R_c	$\frac{\rho_c u_c a^2 d}{y_0}$	moles/m^2/s

for each dissolved species:

$$\alpha^f_{B_1}=k'_{B_1}/k_{B_1}, \tag{22}$$

$$\alpha^f_{B_2}=k'_{B_2}/k_{B_2}, \tag{23}$$

$$\alpha^b_{B_1}=\nu'_{B_1}/\nu_{B_1}, \tag{24}$$

and

$$\alpha^b_{B_2}=\nu'_{B_2}/\nu_{B_2}. \tag{25}$$

The equilibrium fractionation factors between calcite and the two dissolved species are given by

$$\alpha^{eq}_{c-B_1}=\alpha^f_{B_1}/\alpha^b_{B_1} \tag{26}$$

and

$$\alpha^{eq}_{c-B_2}=\alpha^f_{B_2}/\alpha^b_{B_2}. \tag{27}$$

At slow growth, the oxygen in calcite derived from dissolved CO_3^{2-} will have an isotopic composition given by $\alpha^{eq}_{c-B_1}$ and the oxygen derived from HCO_3^- will have a composition given by $\alpha^{eq}_{c-B_2}$.

Before we can solve for the net detachment rate $\overline{\nu}_{B'}$, we need expressions for $P_{B'_1}$ and $P_{B'_2}$; i.e., the distribution of heavy isotopic species adsorbed on the mineral surface. Here we follow the approach of Nielsen et al. (2012), and assume the isotopic composition of each species at kink sites is the same as the isotopic composition of the crystal bulk. This leads to

$$P_{B'_1}=r^*_cP_{B_1} \tag{28}$$

and

$$P_{B'_2}=r^*_c\theta P_{B_1}. \tag{29}$$

The net rate of isotopically heavy carbonate and bicarbonate ion uptake at kink sites on the calcite surface can now be written in terms of the kinetic fractionation factors:

$$u_{B'}=\overline{k}_{B'}[B_1]P_A-\overline{\nu}_{B'}r^*_cP_{B_1}, \tag{30}$$

where the effective attachment rate coefficient takes the form

$$\overline{k}_{B'}=3r_w(\alpha^f_{B_1}k_{B_1}\alpha_{B_1-w}+\phi\alpha^f_{B_2}k_{B_2}\alpha_{B_2-w}) \tag{31}$$

and the effective detachment rate coefficient takes the form

$$\overline{\nu}_{B'}=\alpha^b_{B_1}\nu_{B_1}+\theta\alpha^b_{B_2}\nu_{B_2}. \tag{32}$$

Combining Eqs. (13), (15), and (30) leads to an analytical expression for the isotopic composition of precipitated calcite:

$$r^*_c=\frac{u_{B'}}{u_B}=\frac{\overline{k}_{B'}[B_1]P_A}{\overline{k}_B[B_1]P_A+(\overline{\nu}_{B'}-\overline{\nu}_B)P_{B_1}}. \tag{33}$$

For all model calculations we use the same growth rate parameters as Wolthers et al. (2011) (Table 2), which are constrained by the *p*H-dependence of calcite growth rates in other studies (e.g., Ruiz-Agudo et al., 2011). The four fractionation factors $\alpha^f_{B_1}$, $\alpha^f_{B_2}$, $\alpha^b_{B_1}$, and $\alpha^b_{B_2}$ are the only parameters that are adjusted to construct model isotope ratio profiles.

4.3.3. Two different model approaches

The simplest approach is to assume that the mass discrimination for HCO_3^- isotopologues is identical to that for CO_3^{2-} isotopologues by stating that $\alpha^f_{B_1}=\alpha^f_{B_2}$ and $\alpha^b_{B_1}=\alpha^b_{B_2}$. We refer to this implementation of the modified Wolthers model as 'Model 1' and the top panel in Fig. 7a shows the model $\Delta^{18}O_{c-w}$ as a function of growth rate for several different values of *p*H. The relationship between $\Delta^{18}O_{c-w}$ and R in the top panel is intuitively satisfying; at slow growth rates, the specified equilibrium fractionation factor is recorded by the growing

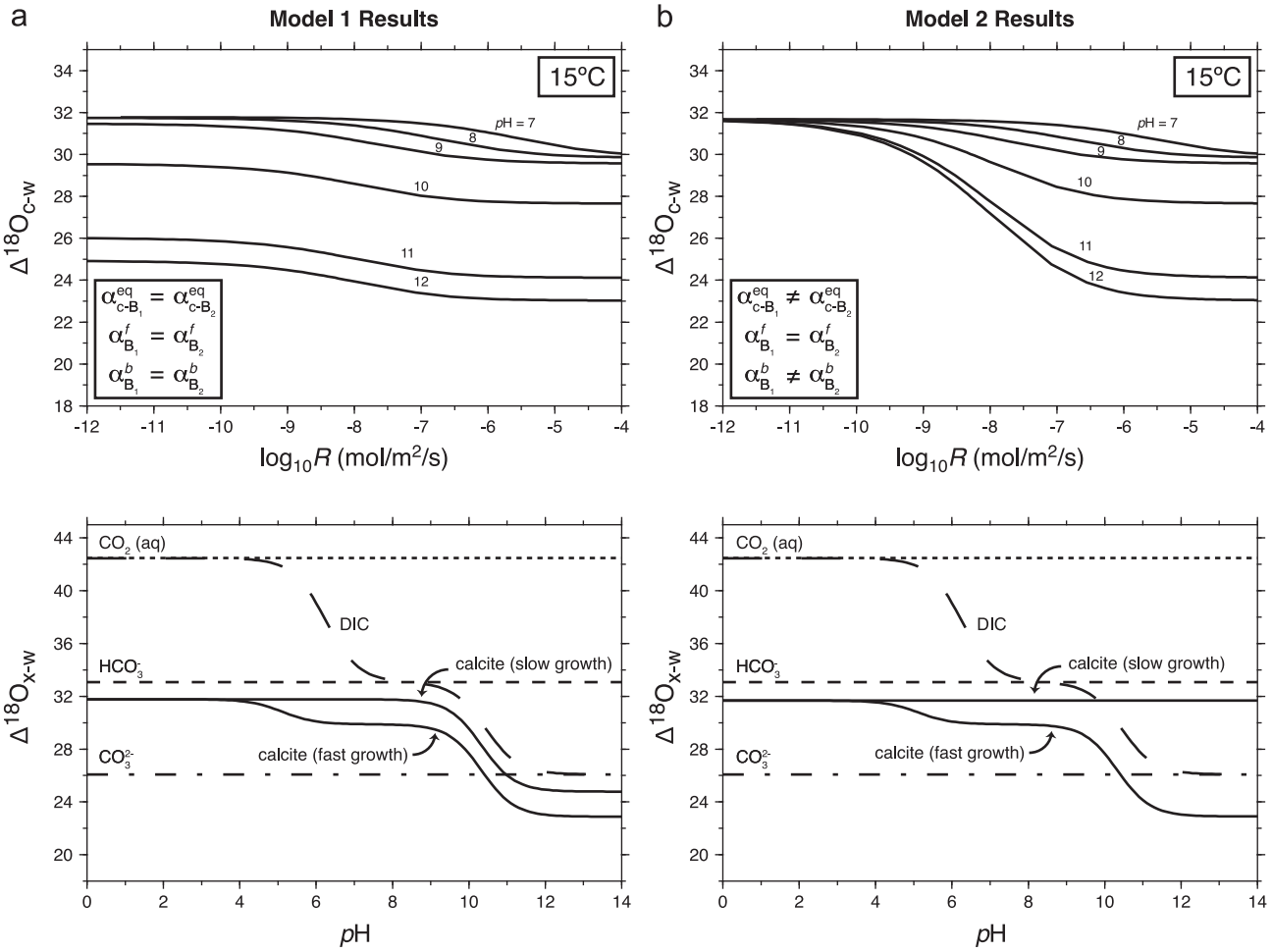

Fig. 7. Model-derived $\Delta^{18}O_{c-w}$ versus growth rate and *p*H at $T = 15$ °C. *Top*: Model 1 predicts a *p*H-dependence to $\Delta^{18}O_{c-w}$ in the slow growth limit whereas Model 2 enforces a *p*H-independent $\Delta^{18}O_{c-w}$ in the slow growth limit. The two models predict identical $\Delta^{18}O_{c-w}$ in the fast growth limit. *Bottom*: The dependence of $\Delta^{18}O_{c-w}$ on *p*H in the slow and fast growth limits. In Model 1, the offset between calcite (slow) and HCO_3^- at $pH < 8$ is given by $\alpha^{eq}_{c-B_2}$ and the offset between calcite (slow) and CO_3^{2-} at $pH > 12$ is given by $\alpha^{eq}_{c-B_1}$. Similarly, the offset between calcite (fast) and HCO_3^- at $pH < 8$ is given by $\alpha^{f}_{B_2}$, whereas the offset between calcite (fast) and CO_3^{2-} at $pH > 12$ is given by $\alpha^{f}_{B_1}$. A similar line of reasoning applies to Model 2, but in this case, $\alpha^{eq}_{c-B_1}$ and $\alpha^{eq}_{c-B_2}$ are not treated independently; they are defined so as to yield the same $\Delta^{18}O^{eq}_{c-w}$.

crystal, given by $\alpha^{eq}_{B_{tot}}$ (the subscript 'tot' refers to the weighted sum of B species), whereas at fast growth a kinetic limit to the isotope fractionations is recorded, given by $\alpha^{f}_{B_{tot}}$. A noteworthy consequence of this formulation is that the α^{eq}_{c-w} in the slow growth limit is *p*H dependent due to the fact that HCO_3^- and CO_3^{2-} are isotopically distinct and the assumption that $\alpha^{eq}_{c-B_1} = \alpha^{eq}_{c-B_2}$ (Eqs. (26) and (27)). The form of this *p*H dependence is shown in the bottom panel of Fig. 7a, where it is observed that the Model 1 $\Delta^{18}O_{c-w}$ is offset from the oxygen isotope composition of $HCO_3^- + CO_3^{2-}$ by a constant value in the limiting cases of extremely slow and extremely fast growth. This output bears similarities to the conceptual model proposed by Zeebe (1999), whereby calcite inherits its oxygen isotope composition directly from DIC. The modified Wolthers model is distinct in that it permits an offset from DIC and it also quantifies the growth rate dependence on $\Delta^{18}O_{c-w}$. Although the main features of Model 1 are consistent with the available data, this implementation may be an inadequate representation of calcite–water fractionation, as several authors have proposed that there should only be one α^{eq}_{c-w} for a given temperature, regardless of *p*H (Watson, 2004; Deines, 2005; Zeebe, 2005).

An alternative approach is to assume that $\Delta^{18}O^{eq}_{c-w}$ is indeed independent of *p*H in the equilibrium limit and use this as an additional constraint. In this case, the equilibrium $\alpha^{eq}_{c-B_1}$ and $\alpha^{eq}_{c-B_2}$ must be defined such that they yield the same α^{eq}_{c-w}. For example, if the equilibrium oxygen isotope composition of calcite falls between that of HCO_3^- and CO_3^{2-} (Fig. 5), then $\alpha^{eq}_{c-B_1}$ must be greater than one while $\alpha^{eq}_{c-B_2}$ must be less than one. In the framework of the Wolthers model, this constraint alone does not satisfy the condition of *p*H independent $\Delta^{18}O^{eq}_{c-w}$ because the ratio of HCO_3^-/CO_3^{2-} participating in the net attachment flux is not equal to the ratio of HCO_3^-/CO_3^{2-} participating in the detachment flux; the forward flux (and its isotopic composition) is given by speciation in the bulk solution whereas the backward flux (and its isotopic composition) is given by speciation at the mineral surface (cf. Table 2 in Wolthers et al., 2011). One way to achieve the desired result without modifying the chemical behavior of the Wolthers model, is to enforce the following statement of calcite–water isotopic equilibrium:

$$\alpha^{eq}_{c-w} r_w = r^{eq}_c = \left(\frac{[^{18}O]}{[^{16}O]}\right)^{eq}_c = \frac{1}{3}\left(\frac{[B']}{[B]}\right)^{eq}_c = \frac{1}{3}\frac{\left(\frac{\overline{k}_{B'}}{\overline{k}_B}\right)}{\left(\frac{\overline{\nu}_{B'}}{\overline{\nu}_B}\right)}. \quad (34)$$

Rearranging, the Model 2 $\overline{\nu}_{B'}$ can be written as

$$\overline{\nu}_{B'} = \frac{\overline{k}_{B'}\overline{\nu}_B}{\overline{k}_B 3 r_w \alpha^{eq}_{c-w}}, \quad (35)$$

Please cite this article as: Watkins, J.M., et al., The influence of kinetics on the oxygen isotope composition of calcium carbonate. Earth and Planetary Science Letters (2013), http://dx.doi.org/10.1016/j.epsl.2013.05.054

where the parameters $\bar{k}_B$ and $\bar{\nu}_B$ are given in Table 3, and $\bar{k}_{B'}$ is given in Eq. (31). The two panels of Fig. 7b show the $\Delta^{18}O_{c-w}$ based on this formulation, hereafter referred to as 'Model 2'. The growth rate dependence in the top panel has similarities to Model 1, but the $\Delta^{18}O^{eq}_{c-w}$ is now fixed at a constant value for all *p*H. The bottom panel shows that the $\Delta^{18}O^{eq}_{c-w}$ is constant, regardless of *p*H.

4.3.4. Comparison between model and data

It is important to note that both Model 1 and Model 2 provide similar outputs over the range of experiment growth rates and nearly identical outputs at *p*H=8.3 (Fig. 7), but for clarity we limit the discussion to the results from Model 2. The curves in Fig. 6 compare Model 2 outputs to existing data at five different temperatures and *p*H values appropriate for comparison to each dataset. For simplicity we assume $\alpha^f_{B_1} = \alpha^f_{B_2}$. Hence there are only two free parameters in this implementation, $\alpha^f_{B_1}$ and $\alpha^{eq}_{c-B_1}$, which are adjusted so as to reconcile the equilibrium $\Delta^{18}O_{c-w} = 28.09$ at 33.7 °C reported by Coplen (2007) and the non-equilibrium $\Delta^{18}O_{c-w}$ values obtained in our catalyzed experiments. The values used to construct Fig. 6 are $\alpha^f_{B_1} = 0.9968$ and $\alpha^{eq}_{c-B_1} = 1.0056$, from which the rest of the α's can be deduced: $\alpha^f_{B_2} = 0.9968$, $\alpha^{eq}_{c-B_2} = 0.9985$, $\alpha^b_{B_1} = 0.9912$, and $\alpha^b_{B_2} = 0.9982$.

Several observations are noteworthy from the information presented in Fig. 6. First, the functional form of the curves is very similar to the model of DePaolo (2011) for Ca isotopes in calcite, but unlike the DePaolo (2011) model, the crossover point from equilibrium to kinetic effects is not an adjustable parameter in this treatment. Second, the model curves agree with the speleothem data of Tremaine et al. (2011), and suggest a slight oxygen isotope disequilibrium at the inferred growth rates given in their electronic annex. Third, the data of Dietzel et al. (2009) are shifted to lower $\Delta^{18}O_{c-w}$ than would be expected for calcites grown in the presence of an equilibrated DIC pool. The observed offset to lower $\Delta^{18}O_{c-w}$ with increasing growth rate may reflect the inability of DIC species to maintain oxygen isotope equilibrium in the growth solution as the equilibrium distribution is perturbed by the precipitation of calcite, or alternatively, as the equilibrium distribution is perturbed by diffusion of CO_2(aq) through a plastic membrane into the growth solution. In either case the presence of carbonic anhydrase in our experiments appears to remove these undesired effects.

If the $\Delta^{18}O^{eq}_{c-w}$ inferred from nature is applicable to our solution compositions, and if the model accurately represents the rate-dependence of $\Delta^{18}O_{c-w}$, then it is unlikely that calcite–water equilibrium has been established in any laboratory experiments. The model curves also illustrate that the temperature-dependence of $\Delta^{18}O_{c-w}$ should not vary significantly at constant precipitation rate, but the slight *p*H dependence may explain why there are several distinct experimentally-determined $\Delta^{18}O_{c-w}$–temperature curves that differ in absolute value but share a similar slope. This same effect may explain why calcite ^{18}O paleothermometry works reasonably well; the temperature dependence is the dominant effect, and growth rate and *p*H effects can be dealt with by limiting species diversity (calcite growth conditions) and making other approximate corrections.

4.3.5. Unresolved issues

By analogy to calcium it is expected that there are kinetic effects on $\Delta^{18}O_{c-w}$ associated with precipitation of calcite from solutions oversaturated by factors of between about 2 and 20 as is typical of experiments and biogenic calcite growth (Tang et al., 2008b; DePaolo, 2011; Nielsen et al., 2012). It is also expected that equilibrium has not been achieved in laboratory crystal growth experiments. There are at least two unresolved issues, however, that affect our understanding of $\Delta^{18}O_{c-w}$ effects and their dependence on temperature and crystal growth rate. First, it is unclear whether the model as formulated properly accounts for the *p*H dependence of kinetic effects as the existing data on experimental calcites grown at high *p*H (not shown) are complicated by isotopic disequilibrium in the bulk solution. Kinetic fractionation due solely to a growth rate dependence would apply if calcite growth from solution involved only the CO_3^{2-} anion, as modeled approximately by Watson (2004) and DePaolo (2011). An additional *p*H dependence would exist if both CO_3^{2-} and HCO_3^- anions were involved in calcite growth.

The second issue concerns the true equilibrium $\Delta^{18}O^{eq}_{c-w}$ and its dependence on *p*H. For the slow growth limit to be consistent with *p*H-independent fractionation, as expected from thermodynamic equilibrium (Watson, 2004; Deines, 2005; Zeebe, 2005), the α's associated with the attachment and detachment fluxes must be significantly different for HCO_3^- than for CO_3^{2-}. In the initial implementation of Model 2 we assumed that $\alpha^f_{B_1} = \alpha^f_{B_2}$, but in future implementations it may be reasonable to relax this assumption. Resolution of the issues surrounding the true $\Delta^{18}O^{eq}_{c-w}$ and α's is part of an ongoing effort, and calcite growth experiments at different *p*H in the presence of CA are being targeted to better constrain the α's assigned to the CO_3^{2-} ion, as well as the *p*H dependence of kinetic effects. As indicated by the time scales required to attain isotopic equilibrium among the DIC species in solution (Fig. 1b), one of the challenges is that it becomes increasingly difficult to precipitate calcite in the presence of an equilibrated DIC pool at high *p*H unless the hydroxylation of CO_2 can somehow be catalyzed.

5. Summary and conclusions

The kinetic effects observed in this study demonstrate how temperature proxies can be sensitive to other environmental variables. For the mineral calcite, kinetic effects arising at the surface of growing crystals can lower the $\Delta^{18}O_{c-w}$ from the equilibrium value by 1–2‰, corresponding to an apparent temperature increase of 4–8 °C. These kinetic effects are unavoidable except for the most slowly-grown minerals, but can be accounted for by adapting the most recent models of ion-by-ion crystal growth. Using growth parameters derived from previous calcite precipitation experiments (e.g., step morphology, attachment/detachment frequency constants, step edge energies, etc.) in conjunction with prescribed equilibrium and kinetic fractionation factors, the model curves plausibly account for a precipitation rate dependence on $\Delta^{18}O_{c-w}$ observed in the various experimental investigations and accommodate the result from slowly precipitated natural cave deposits at 33.7 °C (Coplen, 2007).

Even after decades of effort, determination of equilibrium isotopic fractionation factors in aqueous systems on laboratory timescales represents a formidable challenge. A better understanding of kinetic effects through careful experiments and theory may not only refine temperature estimates derived from carbonate-bearing soils, caves, and ocean sediments, but may provide new opportunities for investigating the role of other environmental variables such as *p*H that influence carbonate growth rates. Our adaptation of the Wolthers et al. (2011) model can be tuned once better constraints are placed on the rate dependence on $\Delta^{18}O_{c-w}$ over a broader range in *p*H. The methods employed in this study can also be extended to "clumped" isotope thermometry, which is based on ^{13}C–^{18}O bond ordering in carbonates. The presence of dissolved CA should accelerate ^{13}C–^{18}O clumped isotope equilibrium in the bulk solution, thereby removing artifacts that are analogous to many of the kinetic oxygen isotope effects discussed here.

Please cite this article as: Watkins, J.M., et al., The influence of kinetics on the oxygen isotope composition of calcium carbonate. Earth and Planetary Science Letters (2013), http://dx.doi.org/10.1016/j.epsl.2013.05.054

Acknowledgments

Alexander Gagnon is credited for suggesting we use carbonic anhydrase in our experiments. Wenbo Yang made the oxygen isotope measurements. Dave Ruddle and Matthew Gonzales helped build the experimental apparatus. We are grateful for discussions with Mariette Wolthers, Aradhna Tripati, Shaun Brown, and Amanda Thomas, as well as comments from two anonymous reviewers. This research was supported by the U.S. Department of Energy, Office of Basic Energy Sciences, Division of Chemical, Biological and Geological Sciences through Lawrence Berkeley National Laboratory and as part of the Center for Nanoscale Control of Geologic CO_2, an Energy Frontier Research Center under contract No. DE-AC02-05CH11231 (LBNL) and Contract No. DE-AC52-07NA27344 (LLNL).

Appendix A. Chemical reactions in the system

Addition of CO_2(g) to an aqueous solution containing dissolved $CaCl_2 \cdot 2H_2O$, $SrCl_2 \cdot 6H_2O$, and NH_4Cl leads to the following chemical relations, which can be used to describe the thermodynamic equilibrium in the carbonate system (Zeebe and Wolf-Gladrow, 2001):

$$CO_2(g) \rightarrow CO_2^*(aq) \tag{A.1a}$$

$$CO_2^*(aq) \overset{K_1^*}{\rightarrow} HCO_3^- + H^+ \tag{A.1b}$$

$$HCO_3^- \overset{K_2^*}{\rightarrow} CO_3^{2-} + H^+ \tag{A.1c}$$

$$Ca^{2+} + CO_3^{2-} \overset{K_{sp}}{\rightarrow} CaCO_3 \tag{A.1d}$$

where $CO_2^*(aq) = CO_2(aq) + H_2CO_3 \approx CO_2(aq)$. Both the addition of CO_2 and the precipitation of $CaCO_3$ drive the pH of the solution downwards. In the previous equations, the K^*'s describe the relative proportions of products and reactants at equilibrium:

$$K_1^* = \frac{(HCO_3^-)(H^+)}{(CO_2^*)} \tag{A.2a}$$

$$K_2^* = \frac{(CO_3^{2-})(H^+)}{(HCO_3^-)} \tag{A.2b}$$

and

$$K_{sp} = (CO_3^{2-})(Ca^{2+}) \tag{A.2c}$$

where the subscript "sp" refers to the solubility product of calcite. Parentheses denote concentrations of chemical species at equilibrium and brackets denote actual or measured concentrations. When there is net growth of $CaCO_3$, the degree of supersaturation with respect to calcite is given by

$$\Omega = \frac{[Ca^{2+}][CO_3^{2-}]}{K_{sp}} \tag{A.3}$$

For solutions with dissolved NH_4Cl, there is an additional reaction that helps buffer the solution pH:

$$NH_4^+ \overset{K_{NH_3}^*}{\rightarrow} NH_3 + H^+ \tag{A.4a}$$

where

$$K_{NH_3}^* = \frac{(NH_3)(H^+)}{(NH_4^+)} \tag{A.4b}$$

All of the K^*'s at 1 atm are functions of salinity and temperature, and the values used throughout the paper are given in Table A1.

Table A1
$pK = -\log_{10} K$ values.

Equilibrium constant	Salinity (‰)	Ionic strength (mol kg^{-1})	5 °C	15 °C	25 °C	35 °C	Reference
pK_1^*	3.6	0.095	6.27	6.19	6.12	6.08	DOE (1994)
pK_2^*	3.6	0.095	10.09	9.97	9.88	9.80	DOE (1994)
$pK_{NH_3}^*$	3.6	0.095	9.92	9.57	9.25	8.96	Clegg & Whitfield (1995)
pK_{sp}	3.6	0.095	7.49	7.48	7.47	7.45	Mucci (1983)
pK_w	3.6	0.095	14.47	14.06	13.70	13.36	DOE (1994)

Appendix B. Charge balance and total alkalinity

Charge balance between all ions in solution gives

$$2[Ca^{2+}] + [Na^+] + [NH_4^+] + [H^+] = [Cl^-] + [HCO_3^-] + 2[CO_3^{2-}] + [OH^-] \tag{B.1}$$

Rearranging so that conservative quantities are on the left-hand side and non-conservative quantities (those whose concentrations may change with T, P, and pH) are on the right-hand side gives

$$\underbrace{2[Ca^{2+}] + [Na^+] - [Cl^-]}_{\text{conservative ions}} = \underbrace{[HCO_3^-] + 2[CO_3^{2-}] + [OH^-] - [H^+] - [NH_4^+]}_{\text{non-conservative ions}} \tag{B.2}$$

Substituting $[NH_4^+] = [NH_3]_{tot} - [NH_3]$, and noting that $[NH_3]_{tot}$ is a conservative quantity, we have

$$\begin{aligned} TA &= \underbrace{2[Ca^{2+}] + [Na^+] - [Cl^-] + [NH_3]_{tot}}_{\text{conservative ions}} \\ &= \underbrace{[HCO_3^-] + 2[CO_3^{2-}] + [NH_3] + [OH^-] - [H^+]}_{\text{non-conservative ions}}, \end{aligned} \tag{B.3}$$

where TA is the total alkalinity, a measurable quantity (cf. Wolf-Gladrow et al., 2007). If we neglect the relatively small $[OH^-]$ and $[H^+]$ terms (~10^{-3} mM and 10^{-6} mM at pH = 8.3, respectively), the right-hand side is identical to the definition of alkalinity used by Lemarchand et al. (2004). Based on the nature of our experiments, changes in TA reflect the addition of Na^+ during autotitration or removal of Ca^{2+} through the precipitation of $CaCO_3$. Assuming $[Cl^-]$ and $[NH_3]_{tot}$ are indeed conserved, the left-hand side of Eq. (B.3) states that any change in TA is due to addition of Na^+ during autotitration or removal of Ca^{2+} during precipitation of $CaCO_3$.

References

Beck, W.C, Grossman, E.L., Morse, J.W., 2005. Experimental studies of oxygen isotope fractionation in the carbonic acid system at 15, 25, and 40 °C. Geochim. Cosmochim. Acta 69 (14), 3493–3503.

Chacko, T., Deines, P., 2008. Theoretical calculation of oxygen isotope fractionation factors in carbonate systems. Geochim. Cosmochim. Acta 72 (15), 3642–3660.

Coplen, T.B., 2007. Calibration of the calcite–water oxygen-isotope geothermometer at Devils Hole, Nevada, a natural laboratory. Geochim. Cosmochim. Acta 71 (16), 3948–3957.

Deines, P., 2005. Comments on "an explanation of the effect of seawater carbonate concentration on foraminiferal oxygen isotopes," by R.E. Zeebe (1999). Geochim. Cosmochim. Acta 69, 787.

Dennis, K.J., Schrag, D.P., 2010. Clumped isotope thermometry of carbonatites as an indicator of diagenetic alteration. Geochim. Cosmochim. Acta 74 (14), 4110–4122.

DePaolo, D.J., 2011. Surface kinetic model for isotopic and trace element fractionation during precipitation of calcite from aqueous solutions. Geochim. Cosmochim. Acta 75 (4), 1039–1056.

Dietzel, M., Tang, J., Leis, A., Köhler, S.J., 2009. Oxygen isotopic fractionation during inorganic calcite precipitation: effects of temperature, precipitation rate and pH. Chem. Geol. 268 (1), 107–115.

Please cite this article as: Watkins, J.M., et al., The influence of kinetics on the oxygen isotope composition of calcium carbonate. Earth and Planetary Science Letters (2013), http://dx.doi.org/10.1016/j.epsl.2013.05.054

Epstein, S., Buchsbaum, R., Lowenstam, H.A., Urey, H.C., 1953. Revised carbonate-water isotopic temperature scale. Geol. Soc. Am. Bull. 64 (11), 1315–1326.

Fantle, M.S., DePaolo, D.J., 2007. Ca isotopes in carbonate sediment and pore fluid from ODP Site 807A: the Ca^{2+}(aq)–calcite equilibrium fractionation factor and calcite recrystallization rates in Pleistocene sediments. Geochim. Cosmochim. Acta 71 (10), 2524–2546.

Gabitov, R.I., Watson, E.B., Sadekov, A., 2012. Oxygen isotope fractionation between calcite and fluid as a function of growth rate and temperature: an *in situ* study. Chem. Geol. 306–307, 92–102.

Ghannam, A.F., Tsen, W., Rowlett, R.S., 1986. Activation parameters for the carbonic anhydrase II-catalyzed hydration of CO_2. J. Biol. Chem. 261 (3), 1164–1169.

Ghosh, P., Adkins, J., Affek, H., Balta, B., Guo, W., Schauble, E.A., Schrag, D., Eiler, J.M., 2006. ^{13}C–^{18}O bonds in carbonate minerals: a new kind of paleothermometer. Geochim. Cosmochim. Acta 70 (6), 1439–1456.

Hoefs, J., 2009. Stable Isotope Geochemistry. Springer, Berlin Heidelberg.

Kim, S.T., O'Neil, J.R., 1997. Equilibrium and nonequilibrium oxygen isotope effects in synthetic carbonates. Geochim. Cosmochim. Acta 61 (16), 3461–3475.

Lachniet, M.S., 2009. Climatic and environmental controls on speleothem oxygen-isotope values. Quat. Sci. Rev. 28 (5), 412–432.

Lemarchand, D., Wasserburg, G.J., Papanastassiou, D.A., 2004. Rate-controlled calcium isotope fractionation in synthetic calcite. Geochim. Cosmochim. Acta 68 (22), 4665–4678.

McCrea, J.M., 1950. On the isotopic chemistry of carbonates and a paleotemperature scale. J. Chem. Phys. 18 (6), 849–857.

Nielsen, L.C., DePaolo, D.J., DeYoreo, J.J., 2012. Self-consistent ion-by-ion growth model for kinetic isotopic fractionation during calcite precipitation. Geochim. Cosmochim. Acta 86, 166–181.

O'Neil, J.R., Clayton, R.N., Mayeda, T.K., 1969. Oxygen isotope fractionation in divalent metal carbonates. J. Chem. Phys. 51, 5547.

Paneth, P., O'Leary, M.H., 1985. Carbon isotope effect on dehydration of bicarbonate ion catalyzed by carbonic anhydrase. Biochemistry 24 (19), 5143–5147.

Pinsent, B.R.W., Pearson, L., Roughton, F.J.W., 1956. The kinetics of combination of carbon dioxide with hydroxide ions. Trans. Faraday Soc. 52, 1512–1520.

Ruiz-Agudo, E., Putnis, C., Rodriguez-Navarro, C.V., Putnis, A., 2011. Effect of pH on calcite growth at constant $a_{ca^{2+}}/a_{co_3^{2-}}$ ratio and supersaturation. Geochim. Cosmochim. Acta 75 (1), 284–296.

Tang, J., Dietzel, M., Böhm, F., Köhler, S.J., Eisenhauer, A., 2008a. Sr^{2+}, Ca^{2+} and $^{44}Ca/^{40}Ca$ fractionation during inorganic calcite formation II: Ca isotopes. Geochim. Cosmochim. Acta 72 (15), 3733–3745.

Tang, J., Köhler, S.J., Dietzel, M., 2008b. Sr^{2+}, Ca^{2+} and $^{44}Ca/^{40}Ca$ fractionation during inorganic calcite formation I: Sr incorporation. Geochim. Cosmochim. Acta 72 (15), 3718–3732.

Tremaine, Darrel M., Froelich, Philip N., Wang, Yang, 2011. Speleothem calcite farmed *in situ*: modern calibration of $\delta^{18}O$ and $\delta^{13}C$ paleoclimate proxies in a continuously-monitored natural cave system. Geochim. Cosmochim. Acta 75 (17), 4929–4950.

Tripati, A.K., Eagle, R.A., Thiagarajan, N., Gagnon, A.C., Bauch, H., Halloran, P.R., Eiler, J.M., 2010. ^{13}C–^{18}O isotope signatures and 'clumped isotope' thermometry in foraminifera and coccoliths. Geochim. Cosmochim. Acta 74 (20), 5697–5717.

Uchikawa, J., Zeebe, R.E., 2012. The effect of carbonic anhydrase on the kinetics and equilibrium of the oxygen isotope exchange in the CO_2–H_2O system: implications on $\delta^{18}O$ vital effects in biogenic carbonates. Geochim. Cosmochim. Acta 95, 15–34.

Urey, H.C., 1947. The thermodynamic properties of isotopic substances. J. Chem. Soc. (Resumed), 562–581.

Usdowski, E., Hoefs, J., 1993. Oxygen isotope exchange between carbonic acid, bicarbonate, carbonate, and water: a re-examination of the data of McCrea (1950) and an expression for the overall partitioning of oxygen isotopes between the carbonate species and water. Geochim. Cosmochim. Acta 57 (15), 3815–3818.

Usdowski, E., Michaelis, J., Böttcher, M.E., Hoefs, J., 1991. Factors for the oxygen isotope equilibrium fractionation between aqueous and gaseous CO_2, carbonic acid, bicarbonate, carbonate, and water (19 °C). Z. Phys. Chem 170, 237–249.

Watson, E.B., 2004. A conceptual model for near-surface kinetic controls on the trace-element and stable isotope composition of abiogenic calcite crystals. Geochim. Cosmochim. Acta 68 (7), 1473–1488.

Wolf-Gladrow, D.A., Zeebe, R.E., Klaas, C., Körtzinger, A., Dickson, A.G., 2007. Total alkalinity: the explicit conservative expression and its application to biogeochemical processes. Mar. Chem. 106 (1), 287–300.

Wolthers, M., Nehrke, G., Gustafsson, J.P., Van Cappellen, P., 2011. Calcite growth kinetics: modeling the effect of solution stoichiometry. Geochim. Cosmochim. Acta 77, 121–134.

Zeebe, R.E., 1999. An explanation of the effect of seawater carbonate concentration on foraminiferal oxygen isotopes. Geochim. Cosmochim. Acta 63 (13), 2001–2007.

Zeebe, R., 2005. Reply to comment by p. deines on "an explanation of the effect of seawater carbonate concentration on foraminiferal oxygen isotopes," by R.E. Zeebe (1999). Geochim. Cosmochim. Acta 69 (3), 789–790.

Zeebe, R.E., 2011. On the molecular diffusion coefficients of dissolved CO_2, HCO_3^-, and CO_3^{2-} and their dependence on isotopic mass. Geochim. Cosmochim. Acta 75 (9), 2483–2498.

Zeebe, R.E., Wolf-Gladrow, D.A., 2001. CO_2 in Seawater, Equilibrium, Kinetics, Isotopes, vol. 65, 2001, Elsevier Science Limited, Amsterdam - Boston - London - New York - Oxford - Paris - San Diego - San Francisco - Singapore - Sydney.

Please cite this article as: Watkins, J.M., et al., The influence of kinetics on the oxygen isotope composition of calcium carbonate. Earth and Planetary Science Letters (2013), http://dx.doi.org/10.1016/j.epsl.2013.05.054